Common Mode and Phase to Ground Voltage Reduction in Back-to-Back Power Converters with Discontinuous PWM

Javier Samanes, *Member, IEEE*, Eugenio Gubia, *Member, IEEE*, Xabier Juankorena, and Carlos Girones

***Abstract*—Discontinuous space vector pulse-width modulation (DSVPWM) techniques are an interesting option for three-phase two-level power converters when efficiency is a key factor. Such is the case of back-to-back (B2B) power converters used mainly in wind energy conversion systems (WECS) and electrical drives. The application of DSVPMWs to B2B converters, increases the common-mode (CM) and phase-to-ground (PG) voltages by a 50%, compared to conventional space vector pulse width modulation (SVPWM7). Higher CM and PG voltages cause bearing currents and insulation stress, which reduce system reliability. In this paper, this problem is addressed and two DSVPWM strategies are presented to reduce the CM and PG voltages in B2B power converters. In the first proposal, the CM and PG are both limited to the same values as the conventional SVPWM7 without introducing additional commutations. In the second proposal, a further modification is added to reduce the CM by 50%, compared to the SVPWM7, although this modulation strategy eventually requires two additional commutations in certain periods. Experimental and simulation results validate the performance of the proposed strategies.**

***Index Terms*—Pulse-width modulation, back-to-back power converter, space vector modulation, common-mode voltage, phase-to-ground voltage, efficiency.**

I. Introduction

WIND energy conversion systems (WECS) and reversible electrical drives are normally connected to the grid through a back-to-back (B2B) two-level power converter [1], as shown in Fig. 1. This conversion structure is formed by the machine side converter, MSC, and the grid side converter, GSC.

Reliability is one of the most important factors in WECS. In modern wind turbines, the generator and the gearbox account for 30% of failures [2], most of which occur in the bearings, with significant downtimes [3]. To lengthen the bearing life, is essential to minimize the current passing through them. This can be achieved by reducing the common-mode voltage peak imposed by the B2B converter [4], shown as v_{CM} in Figure 1. Another issue that needs to be addressed is the reduction of partial discharges through the machine wound insulation, which could compromise its durability [5]. To achieve this goal, the maximum phase-to-ground voltage, v_{PG}, imposed by the power converter should be studied carefully and limited, given that, due to the wave transmission through the cable, the voltage amplitude at the machine terminals can be doubled. This peak can be reduced by limiting the maximum voltage produced by the B2B converter and the use of *dv/dt* filters. To this end, the SVPWM7 is traditionally used in both GSC and MSC with synchronized switching carriers. In this way v_{CM} and v_{PG} are limited to $\pm$2E/3 [6], where E is the DC-bus voltage. v_{CM} can be further reduced to $\pm$E/3 [4], termed SVPWM7 common-mode voltage reduction (SVPWM7–CMVR). As an alternative, the implementation of active zero SVPWM (AZSVPWM) [7] in MSC with SVPWM7 in GSC has been discussed in [8] to also obtain a v_{CM} equal to $\pm$E/3. However, with AZSVPWM, the harmonic distortion is greatly increased. v_{CM} can even be eliminated by coordinating the modulations in GSC and MSC [9], but in this case the modulation in GSC is also modified affecting grid code compliance. All these modulations have the same number of commutations per switching period as the SVPWM7, and are based on the modification of the switching instants, so no improvement in efficiency is obtained.

With regard to WECS, efficiency is a key factor; a 1% improvement in the efficiency of a power converter can result in millions of dollars of savings at a wind farm level [1]. To limit the power losses in high-power converters, the switching frequency is decreased and the sampling frequency

Manuscript received February 7, 2019; revised March 26, 2019 and July 5, 2019; accepted September 5, 2019. This work has been supported by the Spanish State Research Agency (AEI) and FEDER-UE under grant DPI2016-80641-R.

J. Samanes and E. Gubia are with the Department of Electrical, Electronic and Communications Engineering and the Institute of Smart Cities (ISC), Public University of Navarre (UPNA), 31006, Pamplona, Spain. The corresponding author is Javier Samanes (e-mail: javier.samanes@unavarra.es).

X. Juankorena and C. Girones are with Ingeteam Power Technology S.A. - Energy, 31621, Sarriguren, Spain.

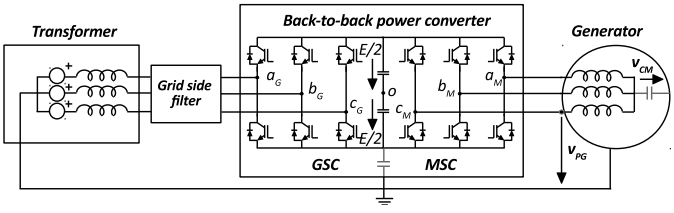

Fig. 1. Typical B2B structure used in WECS and electrical drives.

is reduced accordingly, creating stability issues [10]. Some of these issues could be overcome if the switching losses were reduced, and consequently, the switching frequency and the sampling frequency could be increased. Additionally, an increase in the switching frequency, would benefit the volume and cost of the grid-side filter. An interesting approach to achieve an improvement in efficiency is the modification of the modulation strategy by using discontinuous SVPWMs (DSVPWMs). The number of commutations can be reduced, thus reducing switching power losses. In this respect, one of the most interesting approaches is the GDSVPWM [11], which avoids any switching in the converter leg with the highest current. With this strategy, it is possible to reduce switching losses to half those of the SVPWM7. Another interesting approach is the DSVPWM3 [12], which is optimized to minimize the differential voltage harmonic content, achieving at the same time a 33% reduction in switching losses. Even though, in general, DSVPWMs present greater differential harmonics than the SVPWM7, at high modulation indexes, such as the ones required in GSC, the harmonic content in both modulations becomes similar [13]. This is a relevant factor, given the fact that the GSC is responsible for grid code compliance [14].

Nevertheless, the application of DSVPWMs to B2B conversion structures brings some challenges with regard to reliability. Recently, in [15], the use of DSVPWMs was analyzed for B2B power converters, resolving one of the reliability issues that may arise: higher currents through the DC-bus. However, there are additional challenges that need to be addressed, if these modulations are to become an alternative to SVPWM7. If DSVPWMs are used in GSC and MSC, v_{CM} and v_{PG} are increased to unacceptable levels, with peaks equal to the entire DC-bus voltage, ±E. These voltage levels represent a 50% in relation to the SVPWM7, critically affecting system reliability.

This article proposes two DSVPWM strategies for the B2B structure to reduce v_{CM} and v_{PG}. Both strategies are based on the synchronization of the switching orders of GSC and MSC, considering the effects of the dead time. With the first strategy, v_{CM} and v_{PG} are limited to ±2E/3, maintaining the efficiency improvement of DSVPWMs. With the second strategy, v_{CM} is limited to ±E/3, but eventually requiring additional commutations. In both cases, the efficiency achieved is greater than that of SVPWM7 and only the modulation in MSC is modified. Experimental results in a 500 kW B2B power converter are provided to validate the modulation strategies.

II. Common-Mode and Phase-to-Ground Voltages

A. Influence of the Switching States

In the B2B power converter shown in Fig. 1 the transformer secondary neutral point and the generator frame are connected to ground [16]. If the grid side filter, the transformer and the generator impedances are balanced, the common-mode voltage, v_{CM}, applied by the power converter to the generator is given, in steady-state, by Eq. 1. The phase-to-ground voltage in the generator phase *i*, v_{PG_i}, is given by Eq. 2.

$$v_{CM} = \frac{(v_{a_M o} + v_{b_M o} + v_{c_M o})}{3} - \frac{(v_{a_G o} + v_{b_G o} + v_{c_G o})}{3} \tag{1}$$

$$v_{PG_i} = v_{i_M o} - \frac{(v_{a_G o} + v_{b_G o} + v_{c_G o})}{3} \tag{2}$$

Where each phase voltage, *a, b* or *c*, is measured with respect to the DC-link mid-point, *o*. The subindex *G* stands for GSC and *M* for MSC. It can be seen that v_{CM} depends on the difference of common-mode voltages of GSC and MSC, and v_{PG_i} depends on the voltage of phase *i* in MSC and the common-mode voltage of GSC. Both equations can be rewritten in terms of the switching states; s_{a_M}, s_{b_M} and s_{c_M} for MSC and s_{a_G}, s_{b_G} and s_{c_G} for GSC. Each switching state, s_i, can be either 1 if the upper switch is closed or -1 if it is open. Consequently, the voltage in each phase is either E/2 or -E/2. By expressing the phase voltages in Eq. 1 and 2, in terms of the switching sates, Eq. 3 and 4 are obtained.

$$v_{CM} = \frac{E}{6}\Big((s_{a_M} + s_{b_M} + s_{c_M}) - (s_{a_G} + s_{b_G} + s_{c_G})\Big) \tag{3}$$

$$v_{PG_i} = \frac{E}{2}\left(s_{i_M} - \frac{(s_{a_G} + s_{b_G} + s_{c_G})}{3}\right) \tag{4}$$

In this way, when opposite zero vectors coexist in GSC and MSC, v_{CM} reaches ±E, which is the worst possible case. The second highest voltages occur when a zero vector matches a differential vector with common-mode voltage of opposite sign; in this case v_{CM} would be equal to ±2E/3. When two differential vectors, with opposite common-mode coexist, v_{CM} is equal to ±E/3, while it changes to 0 when two vectors with the same common-mode are modulated simultaneously. PG voltage, v_{PG_i}, is equal to ±E when a zero vector of GSC coexists with a voltage in the converter leg *i* of MSC with opposite sign. This occurs when the zero vector in MSC is larger than the one in GSC. It is equal to ±2E/3 when the leg voltage in MSC coexists with a differential vector of opposite common-mode in GSC. It is ±E/3 if the leg voltage in MSC matches a differential vector in GSC with the same common-mode sign. And finally, v_{PG_i} is 0 when the leg voltage *i* in MSC matches a zero vector with the same CM sign.

B. DSVPWM in B2B VSC

In this section, the worst cases in v_{CM} and v_{PG_i} are analyzed when the-state-of-the-art DSVPWMs are applied to a B2B conversion structure. At first, a brief discussion on the implementation of the space vector modulation is provided, as it is extensively used throughout this paper. The well-known space vector diagram of a two-level three-phase power converter is shown in Fig. 2. These vectors are classified into differential vectors (v_1, ..., v_6), and zero vectors (v_0 and v_7). To synthesize the reference voltage, v_{ref}, required by the controller, the vectors are applied in a sequence that guarantees that only one converter leg is switched in any vector transition.

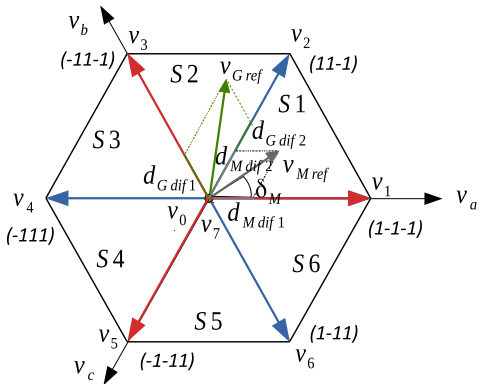

Fig. 2. Space vector diagram with the eight possible switching states of a two-level power converter and the representation of the reference vectors of the machine and grid side converters; v_{Mref} and v_{Gref}.

Each switching period starts with a negative zero vector, v_0, followed by the first differential vector, v_{dif1}, the adjacent red vector to v_{ref}, as shown in Fig. 2. v_{dif1} is followed by v_{dif2}, the adjacent blue vector, and finally, the positive zero vector, v_7:

$$v_0 \rightarrow v_{dif1} \rightarrow v_{dif2} \rightarrow v_7 \rightarrow v_{dif2} \rightarrow v_{dif1} \rightarrow v_0$$

The duty cycle of each vector is denoted by d: d_{z0} is the duty cycle of v_0, d_{dif1} is the duty cycle of v_{dif1} and d_{dif2} the one of v_{dif2}. To compute the duty cycles for the active vectors, the following expressions are used:

$$d_C = m\frac{\sqrt{3}}{2}sin(S\pi/3 - \delta) \tag{5}$$

$$d_A = m\frac{\sqrt{3}}{2}sin\left(\delta - (S-1)\pi/3\right) \tag{6}$$

where d_C is the closest differential vector to the reference vector in the clockwise direction and d_A in the anticlockwise direction. S is the sector number, m is the modulation index, computed as the magnitude of the reference voltage, v_{ref}, divided by E/2, and δ is its angle in relation to space vector v_1, as represented in Fig. 2. In every odd sector, d_{dif1} equals d_C and d_{dif2} equals d_A, while in every even sector d_{dif1} equals d_A and d_{dif2} equals d_C.

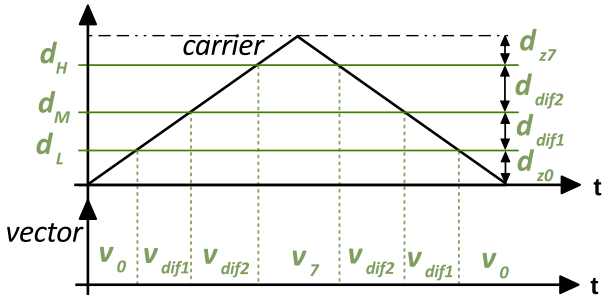

Fig. 3. Space vector implementation of the modulation.

The application instants of these vectors can be obtained from the comparison of three auxiliary duty cycles: low (d_L), medium (d_M), and high (d_H), with a triangular carrier wave, as shown in Fig. 3. The auxiliary d_L, d_M and d_H are computed according to Eq. 7-9.

$$d_L = d_{z0} \tag{7}$$

$$d_M = d_{z0} + d_{dif1} \tag{8}$$

$$d_H = d_{z0} + d_{dif1} + d_{dif2} \tag{9}$$

It should be noted that, in this implementation of the space vector modulation, if the carrier wave is greater than d_H, the positive zero vector, v_7 (1,1,1), is applied and if it is lower than d_L, the negative zero vector is applied, v_0 (-1,-1,-1). In this way, if d_L is equal to zero or d_H is equal to 1, v_0 or v_7, respectively, are eliminated from the sequence, implementing DSVPWMs.

With DSVPWM v_{CM} and v_{PG_i} reach $\pm$E when the reference vector of GSC, v_{Gref}, and the reference vector of MSC, v_{Mref}, have largely different magnitude and the power converters are using a different zero vector. For instance, let us suppose that the reference vectors are in the positions shown in Fig. 2. v_{Mref}, is in the first sector (S1), while v_{Gref}, is located in the second sector (S2), with v_{Gref} having greater magnitude than v_{Mref}. Depending on the discontinuous modulation used, MSC can be using a different zero vector than GSC, as the reference vectors are placed in adjacent sectors. This situation described is shown in Fig. 4 (a) in terms of the corresponding switching states of GSC and MSC. The resulting v_{CM} and v_{PG_a} are also computed. In this figure, MSC is using the positive zero vector, while GSC is using the negative zero vector. If the zero duty cycles are large enough, as in the case shown, v_{CM} is equal to E. v_{PG_a} is also equal to E, because the negative zero vector in GSC, with a CM of -E/2, is added to a leg voltage of E/2 in phase a of MSC.

This higher CM and PG voltages, if compared to SVPWM7 or SVPWM7–CMVR, can lead to premature failures in bearings and insulation [17], so coordinated modulations for B2B structures should be developed.

III. Proposed DSVPWM Strategies

To improve the phase-to-ground and common-mode voltages of DSVPWMs for B2B VSCs, two modulation strategies are proposed in which the modulation of MSC is modified, depending on the vectors used in GSC and their duty cycles. The modulation in GSC is unaltered, therefore grid code compliance is not compromised. In the first proposal, a master–slave implementation, DSVPWM–MS, is proposed to avoid the worst case in both, v_{CM} and v_{PG}, reducing them to $\pm$2E/3, as for SVPWM7, without introducing additional commutations. In the second proposal, DSVPWM–CMVR, v_{CM} is further reduced to $\pm$E/3, as for the SVPWM7–CMVR, however in this case additional commutations are required in certain switching periods.

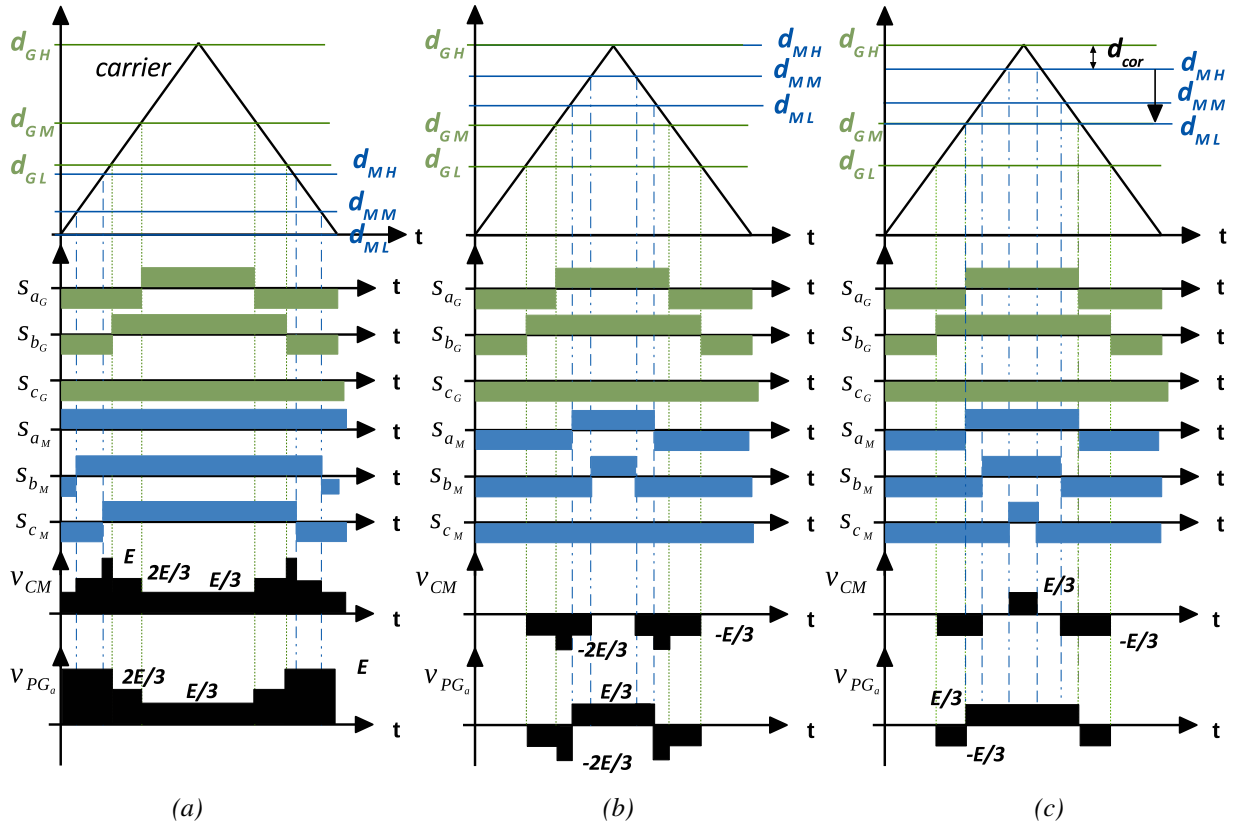

Fig. 4. CM and PG voltages depending on the switching states of GSC (with v_{ref} in S2) and MSC (with v_{ref} in S1) and different modulation strategies: DSVPWM (a), DSVPWM forcing MSC to use the same zero vector as GSC (DSVPWM–MS) (b) and DSVPWM in GSC and common mode voltage reduction in MSC (DSVPWM–CMVR) (c).

A. DSVPWM–MS: Limiting v_{CM} and v_{PG} to $\pm$2E/3

In Section II, it has been identified that v_{CM} reaches a peak of $\pm$E whenever MSC and GSC use, at the same instant, opposite zero vectors, as shown in Fig. 4 (a). With regard to v_{PG}, $\pm$E is reached whenever the zero vector of GSC is not matched by the same zero vector in MSC. Taking into account both premises, v_{CM} and v_{PG} can be simultaneously reduced to $\pm$2E/3 by introducing in MSC the same zero vector as for GSC. Both power converters use the same carrier wave, so v_{PG} will never reach $\pm$E as long as the zero vector in MSC is larger than the one in GSC. This condition is also a requirement for the SVPWM7 to avoid $\pm$E instances when the fundamental frequencies of the GSC and the MSC are different.

The zero vector used by MSC is determined by Eq. 10. If the lowest duty cycle of GSC, d_{GL} is greater than 0, meaning that GSC is using v_0, MSC is forced to use the same vector. This means that the whole zero duty cycle in MSC, d_{Mz}, will be assigned to the negative zero vector of MSC d_{Mz0}. Otherwise, MSC uses v_7, the same zero vector as GSC.

$$d_{Mz0} = \begin{cases} d_{Mz} & \text{if } d_{GL} > 0 \\ 0, & \text{otherwise} \end{cases} \tag{10}$$

This condition is verified during each sampling period, and the duty cycles of MSC (d_{ML}, d_{MM}, d_{MH}) are calculated accordingly. As an example, in Fig. 4 (a) and (b), the duty cycles of DSVPWM and DSVPWM–MS for the reference vectors of Fig. 2 are shown. In this case, MSC is forced to use the same zero vector as GSC by imposing Eq. 10 in every sampling period. With this strategy, the peak of v_{CM} and v_{PG} is effectively reduced to $\pm$2E/3. Moreover, no additional commutations are introduced, so the whole B2B structure presents 8 commutations per switching period instead of 12 with SVPWM7. As a drawback, neither GDSVPWM nor DSVPWM3 can be used in MSC, as the zero vector is conditioned to be equal to the one in GSC.

B. DSVPWM–CMVR: Limiting v_{CM} to $\pm$E/3

With DSVPWM–MS the same peak in v_{CM} and v_{PG} is achieved as with SVPWM7, while reducing the power losses. However, with SVPWM7–CMVR the peak of v_{CM} is reduced to $\pm$E/3. To achieve the same voltage levels, a modification to the DSVPWM–MS, denoted as DSVPWM–CMVR, is proposed as follows.

Revisiting the common-mode voltage in Fig. 4 (b), it can be noted that v_{CM} reaches its maximum of $\pm$2E/3 only when a zero vector coincides with a differential vector, in the other converter, that has a common-mode with the opposite sign. If Fig. 4 (b) is studied carefully, it can be concluded that this occurs when d_{ML} is greater than d_{GM}. Similarly, this situation would also occur when d_{MH} is lower than d_{GM}. In

both cases, v_{CM} reaches ±2E/3 because the time duration of the zero vector in MSC is greater than the sum of the durations of the zero and the adjacent differential vector in GSC.

To avoid these situations, in a similar way to the SVPWM7-CMVR, the three duty cycles in MSC can be modified by the difference between the zero and differential vectors of GSC and MSC, denoted by d_{cor} in Fig. 4 (b). This action only affects the duration of the zero vectors and not the differential ones. In the case shown in Fig. 4 (b), d_{cor} is set equal to the difference between d_{ML} and d_{GM}. If d_{ML} is reduced by d_{cor}, meaning that the application time of v_0 in MSC is decreased, the -2E/3 peak in the common-mode voltage is eliminated. The other zero vector, v_7 in this case, has to be increased, as represented in Fig. 4 (c), to avoid the modification of the modulated reference vector. As a result, two additional commutations are introduced in this particular switching period. Whenever the modulation needs to be corrected, MSC has 6 commutations per switching period, resulting in 10 in the entire B2B structure. However, this correction is only applied when the conditions in Eq. 11 and 12 are met.

$$\begin{aligned} if(d_{ML} > d_{GM}) &\rightarrow d_{cor} = d_{ML} - d_{GM} \\ &\rightarrow d_{Mz0} = d_{Mz} - d_{cor} \end{aligned} \tag{11}$$

$$\begin{aligned} if(d_{MH} < d_{GM}) &\rightarrow d_{cor} = d_{GM} - d_{MH} \\ &\rightarrow d_{Mz0} = d_{cor} \end{aligned} \tag{12}$$

Once the required corrections specified in Eq. 11 and 12 are applied, the duty cycles are easily recalculated with the expressions in Eq. 7, 8 and 9. In Fig. 4 (c) the proposed modifications have been applied, showing that the peak of v_{CM} is reduced to ±E/3. The number of times in which the correction needs to be used varies depending on the DSVPWM used in GSC, as analyzed in Section IV. For the particular situation represented in Fig. 4 (c), v_{PG} is also limited within ±E/3, however, during the fundamental period, it will reach ±2E/3, so both v_{CM} and v_{PG} are equal to the SVPWM7–CMVR with significant reduction in switching losses. The proposed modulation strategy does not imply a high computational cost in any commercial digital signal processor (DSP) used in high power converters, as it is based on the evaluation of the simple conditions expressed in Eq. 10, 11 and 12.

C. Effect of the dead time

The implementation of dead time, t_d and its effect on the output voltage of a given phase x is shown in Fig. 5. It can be seen that, if the intersection of duty cycle, d_i, with the carrier wave implies a commutation in phase leg x, then the voltage imposed in that phase, and therefore the duration of the new vector, is modified depending on the polarity of the phase current. This can create voltage spikes in the common-mode voltage when DSVPWM?CMVR is used, as it is based on modifying the application instants of the MSC vectors depending on the duty cycles of GSC. If a mismatch

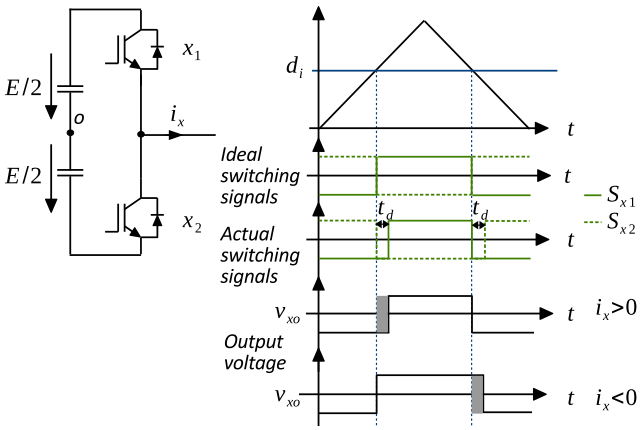

Fig. 5. Output voltages in a given phase taking into account the effect of the dead time.

occurs between the theoretical switching instant and the actual switching instant, the sole application of Eq. 11 and 12 will not eliminate voltage spikes in v_{CM} with a magnitude equal to ±2E/3.

The dead time can be compensated by readjusting the duty cycles depending on the current polarity [18], however, this strategy is not always valid. When the current is close to zero, the dead time compensation can create an even higher error in the applied reference vector due to the existing ripple in the converter current, which may change the actual current polarity at the switching instant. For this reason, the compensation strategy is normally disabled when the converter current is close to zero. To avoid such peaks of ±2E/3 when the dead time compensation is disabled with DSVPWM-CMVR, Eq. 13 and 14 are applied in MSC:

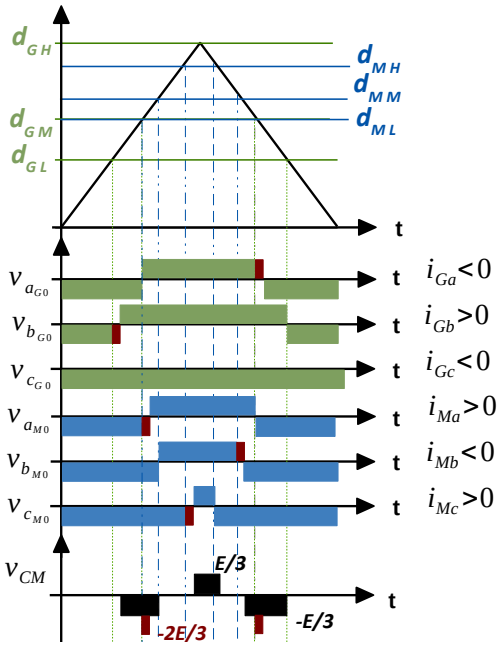

Fig. 6. Real output voltages for the B2B structure considering the dead time effect.

$$if(d_{ML} > d_{GM}) \rightarrow d_{cor} = d_{ML} - d_{GM} + d_d \\ \rightarrow d_{Mz0} = d_{Mz} - d_{cor} \quad (13)$$

$$if(d_{MH} < d_{GM}) \rightarrow d_{cor} = d_{GM} - d_{MH} + d_d \\ \rightarrow d_{Mz0} = d_{cor} \quad (14)$$

where d_d is the dead time duty cycle, defined as t_d/T_s, T_s being the sampling period. epending on the current polarity, Eq. 13 and 14 may create over-compensation, however, they do guarantee that when dead time compensation is disabled, v_{CM} will not reach $\pm$2E/3.

The dead time effect on the common–mode voltage imposed by the B2B conversion structure, v_{CM}, is illustrated in Fig. 6. The same case represented in Fig. 4 (c) is considered, but in this occasion, the real voltages in each phase with respect to the DC-bus mid–point are shown. As it can be seen, depending on the current polarity the actual voltage is deviated from the ideal voltage imposed by the modulator, and consequently, voltage spikes equal to $\pm$2E/3 appear. However, from this figure, it becomes clear that if the additional correction described in Eq. 13 is used, d_{ML} is reduced by d_d and the voltage spikes created by the dead time are eliminated.

IV. Switching Losses of the Proposed DSVPWMs

The main reason for using DSVPWMs in B2B power converters is the efficiency improvement. The previous section, established that the proposed modulations effectively limit v_{PG} and v_{CM}. Moreover, as GSC has a modulation index close to unity, DSVPWM present a reduced THD. However, the proposed modulations for B2B structures, have some differences with those applied to a single power converter and for this reason, an analysis of the switching losses is performed. The switching power losses of SVPWM7, are compared to those of the proposed DSVPWM–MS and DSVPWM–CMVR. The achievable improvement in efficiency with the proposed modulations depends on the modulation in GSC. Two different DSVPWM are tested for GSC: GDSVPWM, used to minimize the switching losses, and DSVPWM3, to improve the grid harmonic content. The space-vector implementation of GDSVPWM and DSVPWM3 is shown in Fig. 7. Each sector is divided into two sub-sectors (I and II), this division determines the transition between the utilization of the positive and the negative zero vector. The DSVPWM–MS does not introduce additional commutations, however, with the DSVPWM–CMVR the modulation in MSC is modified if the conditions in Eq. 11 and 12 are met. Therefore, each time one of these conditions is met, two additional commutations per switching period are introduced. However, depending on the modulation used in GSC, the modulation in MSC needs to be modified a different number of times to maintain v_{CM} within $\pm$E/3. To understand this, in Fig. 8 the duty cycles of the vectors of GSC and MSC are shown for the modulation DSVPWM–CMVR and two different modulations in GSC. In Fig. 8 (a), GSC uses the GDSVPWM, in Fig. 8 (b) it uses the DSVPWM3. The duty cycles shown in Fig. 8 correspond to a modulation index

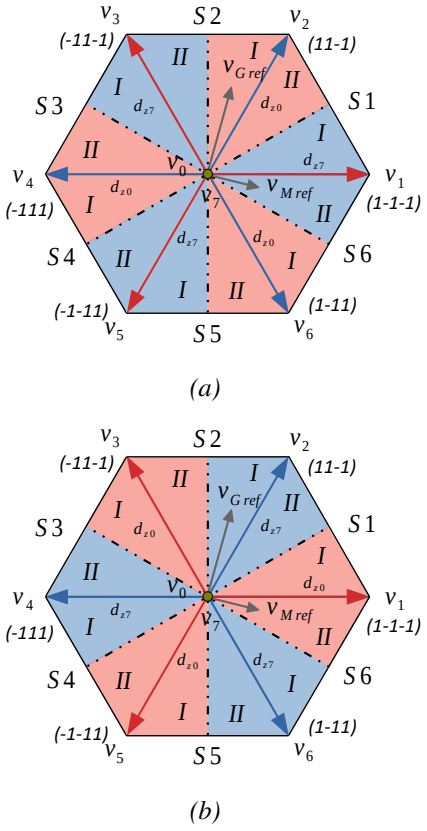

Fig. 7. Implementation of the GDSVPWM with unity power factor (a) and DSVPWM3 (b).

in GSC of 1 and a frequency of 50 Hz, while in MSC the modulation index is 0.4 and the frequency is 11 Hz. Therefore the reference vectors of GSC and MSC are not synchronized. Each time that d_{ML} is other than 0 and, simultaneously, d_{MH} is other than 1, the corrections of Eq. 11 and 12 are being applied. In Fig. 8 (a) it can be seen that MSC is using the correction in every sampling period, applying both zero vectors, to avoid common-voltages of $\pm$2E/3, while in Fig. 8 (b) the correction is used only in a few sampling periods.

To better understand this difference, let us consider the situation shown in Fig. 7 (a) and (b), with $v_{G_{ref}}$ in S2-I and $v_{M_{ref}}$ in S6-II. This instant is marked with the vertical dashed line in Fig. 8. With the GDSVPWM in GSC, Fig. 8 (a), zero vector v_0 is used. At the same time, in order to avoid $\pm$E peaks in both v_{CM} and v_{PG}, MSC is forced to apply the same zero vector v_0. As the modulation index in MSC is lower than in GSC, d_{ML} would be greater than d_{GM}, given that d_{Gdif1}, the duty cycle of v_3, is small, as shown in Fig. 7 (a). The correction in MSC has to be applied in every sampling period, forcing the B2B VSC to commute 10 times in every switching period. In contrast, with the modulation DSVPWM3 in GSC, few corrections are required. As can be seen in Fig. 7 (b), zero vector v_7 is used in GSC at the same instant considered. MSC is also forced to use v_7, but as duty cycle d_{Gdif1} is small, d_{MH} is almost never lower than d_{GM}. In this way, the switching power losses depend on the modulation used, but also on the modulation index in MSC.

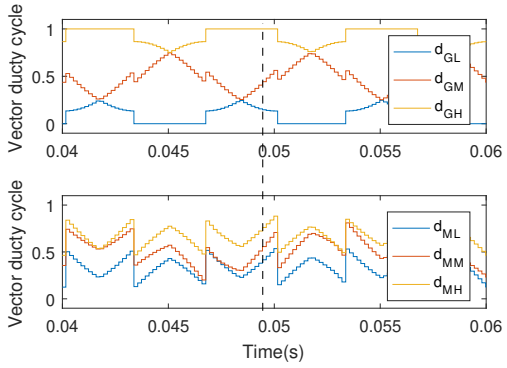

(a)

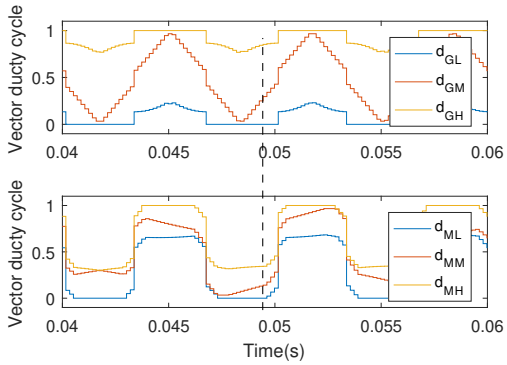

(b)

Fig. 8. Duty cycles of GSC and MSC for the modulation DSVPWM–CMVR using in GSC GDSVPWM (a) and DSVPWM3 (b).

To gain an overall idea of the switching losses, the mean switching power losses are computed for a 500 kW B2B power converter using *Matlab Simpower Systems*, for six different modulations:

- SVPWM7-CMVR: taken as the reference power losses.
- GDSVPWM in GSC and MSC.
- GSC with GDSVPWM and MSC with both GDSVPWM–MS and GDSVPWM–CMVR.
- GSC with DSVPWM3 and MSC with both DSVPWM–MS and DSVPWM–CMVR.

The switching power losses are computed through a S-function in Matlab, in which the IGBT turn-on losses, E_{on}, turn-off losses, E_{off}, and the diode reverse recovery losses, E_{rr}, are calculated for the IGBTs Fuji 6MBI450U-170, the same ones used in the experimental set-up. E_{on}, E_{off} and E_{rr} are computed through 3 cubic polynomials adjusted from the manufacturer's data-sheet:

$$E(I_c) = a_0 I_c^3 + a_1 I_c^2 + a_2 I_c + a_3 \tag{15}$$

where I_c is the collector current. The coefficients for the three polynomials are given in Table I. The energy lost calculated through these polynomials is converted to power using the typical rise and fall times provided in the data-sheet.

As GSC is connected to the grid, it has an almost constant modulation index, that is set equal to 1.1 for the simulations. In contrast, the MSC modulation index has been varied, from

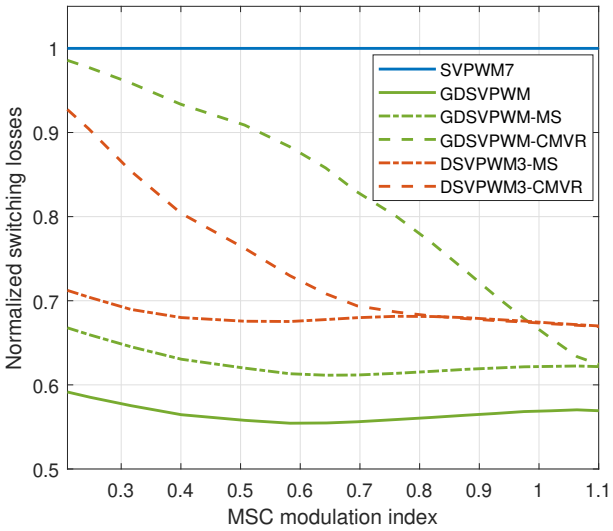

Fig. 9. Normalized switching losses for different modulations: GDSVPWM in both GSC and MSC, GSC with GDSVPWM and MS in MSC (GDSVPWM–MS), GSC with GDSVPWM and CMVR in MSC (GDSVPWM–CMVR), GSC with DSVPWM3 and MS in MSC (DSVPWM3–MS) and at last GSC with DSVPWM3 and CMVR in MSC (DSVPWM3–CMVR).

0.2 to 1.1 in the analysis performed, increasing the power with the modulation index. In this way, the behavior of a generator in a wind turbine is replicated. As the wind speed is higher, the generator rotates faster, generating more power and increasing its voltage. GSC and MSC have different fundamental frequencies, so the power losses are averaged for the minimum common multiple of both fundamental periods. These averaged switching losses are normalized in relation to the losses obtained with the SVPWM7, and represented in Fig. 9, against different modulation indexes in MSC. At low modulation indexes the utilization of CMVR increases the power losses in relation to the proposed master–slave (MS) implementation, because the duty cycle of the zero vector in MSC is large and Eq. 11 and 12 need to be applied. CMVR combined with GDSVPWM has greater switching power losses than their application to DSVPWM3, despite the minimization of the switching losses in GSC. This is caused by the additional corrections required in MSC to reduce v_{CM} to $\pm$E/3 with GDSVPWM. At higher modulation indexes, fewer corrections are required, the power losses of GDSVPWM–CMVR and DSVPWM3–CMVR are reduced, but still the later remains superior, up to a modulation index close to 1.. As DSVPWM3 has a better harmonic content than GDSVPWM, in overall terms, the utilization of DSVPWM3 in

TABLE I
COEFFICIENTS FOR THE SWITCHING LOSS CALCULATION

	a_0	a_1	a_2	a_3
E_{on}	6×10^{-7}	-5.493×10^{-4}	0.3304425	-0.2199956
E_{off}	9×10^{-7}	-9.196×10^{-4}	0.5857601	-3.0652022
E_{rr}	1×10^{-7}	-1.4777×10^{-3}	0.8579511	-4.9736532

Fig. 10. Test bench used for the validation of the proposed modulation strategies.

GSC, with either MS or CMVR, is preferable to the utilization of GDSVPWM. For comparison purposes, the power losses for the conventional GDSVPWM are also represented in Fig. 9

Both, DSVPWM3-MS and DSVPWM3–CMVR make it possible to significantly reduce the power losses, with the same phase-to-ground and common-mode voltages than SVPWM7 and SVPWM7–CMVR, respectively.

V. Experimental Results

The two modulations presented in this work overcome the limitations of DSVPWMs in terms of v_{CM} and v_{PG}. Both have been validated in the experimental set-up of Fig. 10; a 500 kW B2B power converter designed for a DFIG wind turbine, with a switching frequency of 2.8 kHz. The DC-bus voltage is equal to 1150 V for a 690 V grid. The dead times are equal to 4 μs.

Three different DSVPWMs are compared; the use of DSVPWM3 in both GSC and MSC, and the use of the proposed DSVPWM3–MS and DSVPWM3–CMVR. The three modulations are compared in terms of v_{CM} and v_{PG}. The modulation index in MSC is 0.3 with a fundamental frequency of 30 Hz. In all the cases tested, both GSC and MSC use the same carrier wave. To compute the CM and PG voltages, the six phase voltages are measured in relation to the DC-bus voltage using the same differential voltage probes. The results obtained are shown in Fig. 11.

Initially, in Fig. 11 (a) GSC and MSC modulate their reference vector independently, using both the DSVPWM3. As expected, and shown in Fig. 4, both v_{CM} and v_{PG} reach maximum peaks of $\pm$E. These peaks are limited to $\pm$2E/3 when the DSVPWM3–MS is applied, Fig. 11 (b). When both power converters are forced to use the same zero vector, the spikes of $\pm$E are eliminated. A further reduction is obtained in the common-mode when DSVPWM3–CMVR is used, Fig. 11 (c). By displacing the zero vectors in MSC when it is required, v_{CM} is confined within $\pm$E/3, while v_{PG} is still limited to $\pm$2E/3. To conclude the analysis of v_{CM}, in Fig. 12 the harmonic spectra of the common-mode voltage is shown for DSVPWM3, DSVPWM3–MS and DSVPWM3–CMVR. According to the experimental results, the reduction of the maximum peaks in v_{CM} brings a reduction in the harmonic spectra below the switching frequency, but has little effect on the harmonic spectra at high frequencies (1 MHz).

The DSVPWM3 is the preferred modulation to be used with CMVR, because it has a better harmonic content than GDSVPWM, with a greater efficiency at low modulation indexes of MSC. In both, DSVPWM3–MS and DSVPWM3–CMVR, the modulation of GSC remains unaltered, so the grid harmonic content is not modified with the changes in the modulation proposed for MSC. Nevertheless, these changes affect the phase differential voltage harmonic content in MSC. For this reason, in Fig. 13, the weighted THD (WTHD) is examined as a function of the modulation index for the two modulations under analysis in MSC: DSVPWM3, DSVPWM3–MS, DSVPWM3–CMVR and are compared to the SVPWM7 and SVPWM7–CMVR. The WTHD is computed for the first 200 harmonics as indicated in Eq. 16.

$$WTHD = \frac{\sqrt{\sum_{i=2}^{200}(V_i/i)^2}}{V_1} \tag{16}$$

Where V_i is the amplitude of order i voltage harmonic and V_1 is the fundamental harmonic amplitude. As shown in Fig. 13, at low modulation indexes, the WTHD of MSC for the DSVPWM3 and DSVPWM3–MS is greater than the one for SVPWM7 and SVPWM7–CMVR, becoming similar at high modulation indexes. However, with the DSVPWM3–CMVR, as both zero vectors are used in MSC at low modulation indexes, the WTHD is reduced. It becomes similar to DSVPWM3–MS at higher modulation indexes, when the conditions expressed in Eq. 11 and 12 are not met, and, consequently, the corrections are not applied.

Finally, in Fig. 14 (a) the grid current is shown when the DSVPWM3 is used in GSC injecting 300 kW, with its harmonic analysis in Fig. 14 (b).

VI. Conclusion

In this paper, the CM and PG voltages of DSVPWMs in back-to-back power converters are analyzed. Two modulation strategies are proposed which provide a performance comparable to the SVPWM7 but with significant efficiency improvements. If GSC and MSC are modulated independently using DSVPWMs, the common-mode and phase-to-ground voltages reach the entire DC-bus voltage. To solve this issue, a modulation is proposed for back-to-back power converters that make it possible to reduce the common-mode and phase-to-ground voltages to $\pm$2E/3. These are the same voltage levels achieved when the conventional SVPWM7 is used in B2B power converters, but reducing the number of commutations per switching period from 12 to 8. The modulation is called DSVPWM–MS, and forces MSC to use the same zero vector as GSC. To further reduce the common-mode voltage to $\pm$E/3, another modulation is proposed that also forces MSC to use the same zero vector as GSC, but requiring the use of both zero vectors in MSC, in some sampling times, to avoid the peaks of $\pm$2E/3. As a result, the number of commutations is increased to 10 only

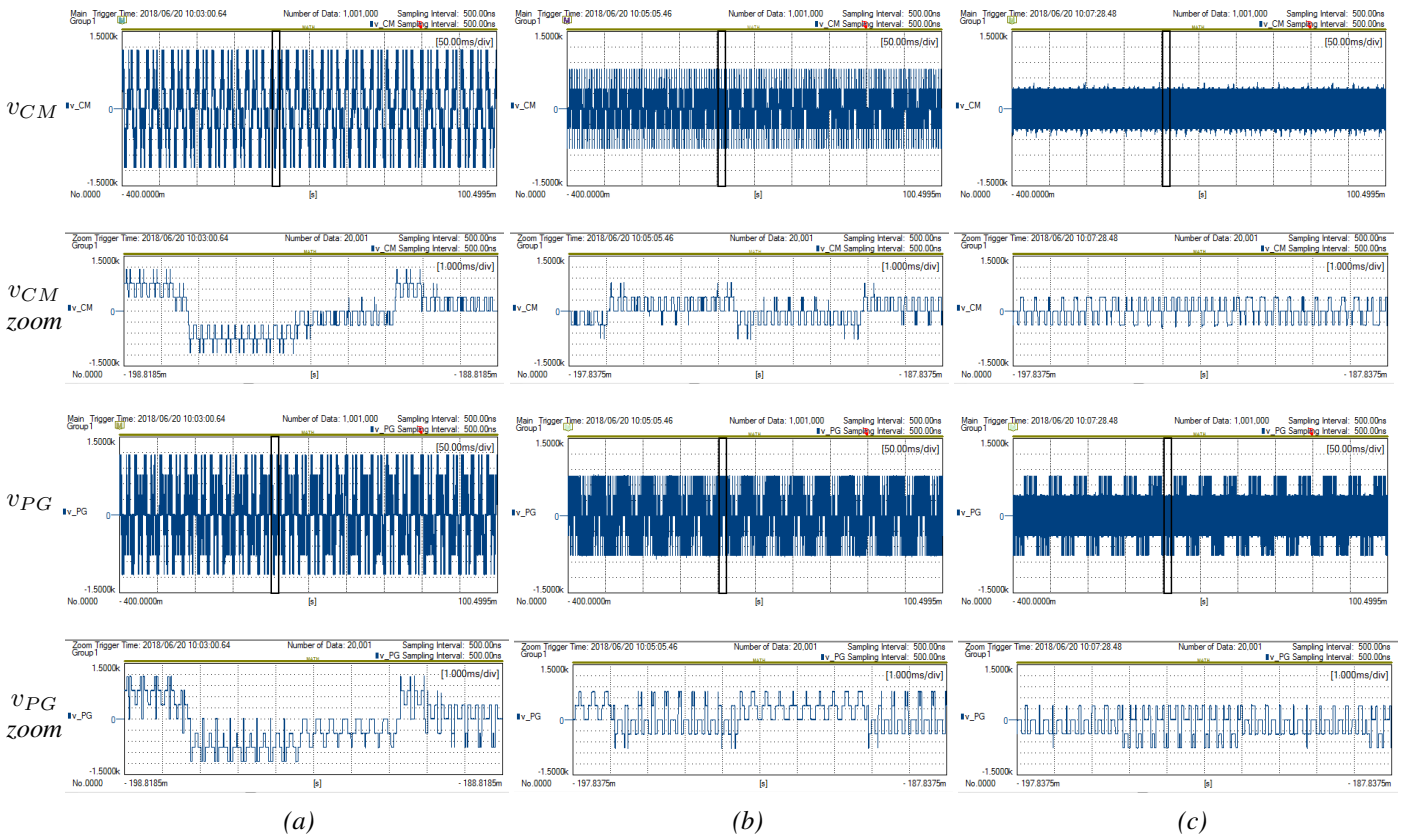

Fig. 11. Comparison of the common-mode and phase-to-ground voltages normalized in relation to the DC-bus voltage for: DSVPWM3 in GSC and MSC (a), DSVPWM3–MS (b) and DSVPWM3–CMVR (c).

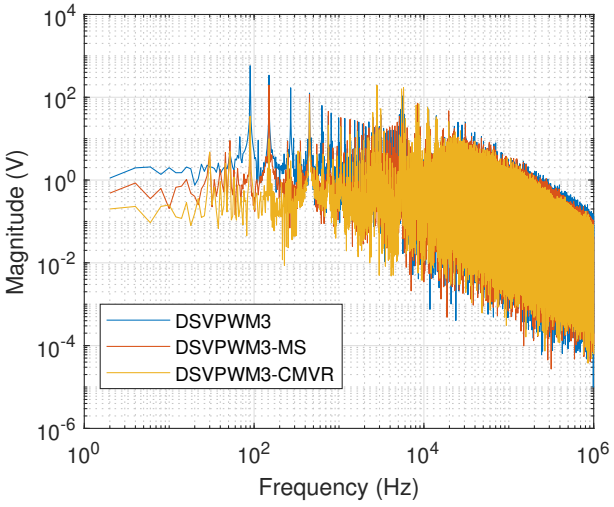

Fig. 12. Common-mode voltage spectra for the DSVPWM3, DSVPWM3–MS and DSVPWM3–CMVR.

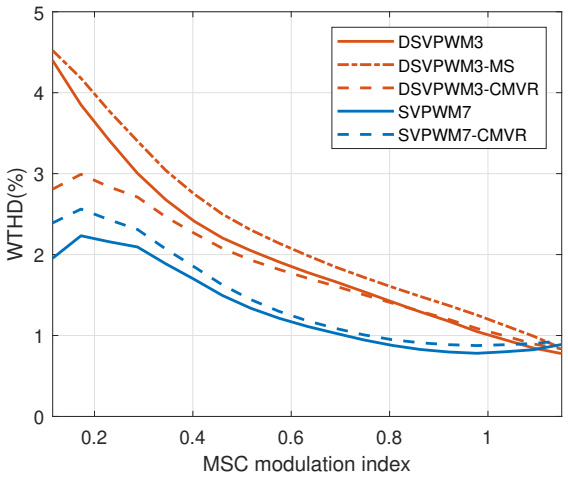

Fig. 13. WTHD for the SVPWM7, SVPWM7–CMVR, DSVPWM3, DSVPWM3–MS and DSVPWM3–CMVR.

in particular switching periods. The number of corrections depends on the modulation used in GSC and the modulation index in MSC. This modulation is termed DSVPWM–CMVR. Considering the efficiency and grid-code compliance, the authors recommend the use of DSVPWM3 in GSC, in combination with the two proposals in MSC. The proposed modulations can reduce the switching power losses by more than a 30% for modulation indexes of more than 0.6 in MSC in grid-connected power converters. Experimental results validate the effectiveness in the reduction of the common-mode and phase-to-ground voltages.

REFERENCES

[1] V. Yaramasu, B. Wu, P. C. Sen, S. Kouro, and M. Narimani, "High-power wind energy conversion systems: State-of-the-art and

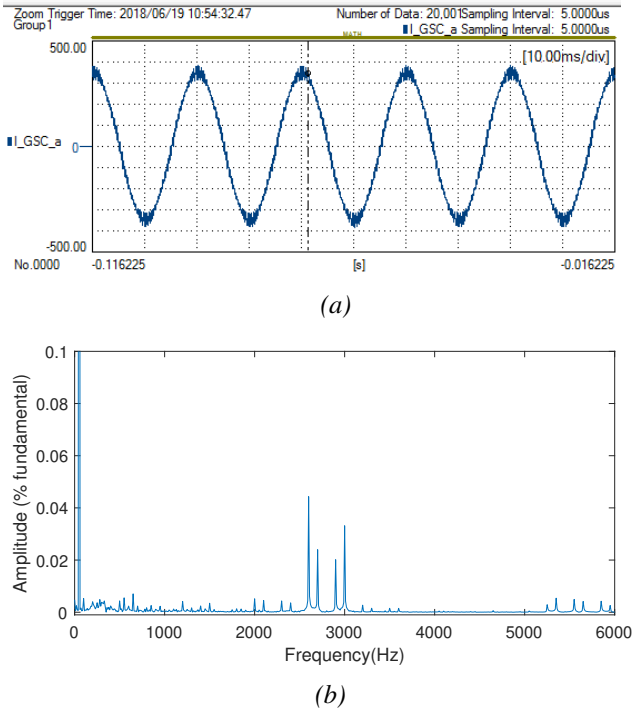

Fig. 14. Grid current waveform (a) and harmonic content (b) for the DSVPWM3.

emerging technologies," *Proc. IEEE*, vol. 103, no. 5, pp. 740–788, 2015.

[2] U. Shipurkar, K. Ma, H. Polinder, F. Blaabjerg, and J. A. Ferreira, "A review of failure mechanisms in wind turbine generator systems," in *Power Electronics and Applications (EPE'15 ECCE-Europe), 2015 17th European Conference on*, pp. 1–10. IEEE, 2015.

[3] H. D. M. de Azevedo, A. M. Araújo, and N. Bouchonneau, "A review of wind turbine bearing condition monitoring: State of the art and challenges," *Renewable and Sustainable Energy Reviews*, vol. 56, pp. 368–379, 2016.

[4] H.-D. Lee and S.-K. Sul, "Common-mode voltage reduction method modifying the distribution of zero-voltage vector in pwm converter/inverter system," *IEEE Transactions on Industry Applications*, vol. 37, no. 6, pp. 1732–1738, 2001.

[5] P. Wang, A. Cavallini, and G. C. Montanari, "Characteristics of pd under square wave voltages and their influence on motor insulation endurance," *IEEE Transactions on Dielectrics and Electrical Insulation*, vol. 22, no. 6, pp. 3079–3086, 2015.

[6] A. M. D. Broe, A. L. Julian, and T. A. Lipo, "Neutral-to-ground voltage minimization in a pwm-rectifier/inverter configuration," in *1996 Sixth International Conference on Power Electronics and Variable Speed Drives (Conf. Publ. No. 429)*, DOI 10.1049/cp:19960975, pp. 564–568, Sep. 1996.

[7] Y.-S. Lai and F.-S. Shyu, "Optimal common-mode voltage reduction pwm technique for inverter control with consideration of the dead-time effects-part i: basic development," *IEEE Transactions on Industry Applications*, vol. 40, no. 6, pp. 1605–1612, 2004.

[8] A. M. Garcia, D. Holmes, and T. Lipo, "Reduction of bearing currents in doubly fed induction generators," in *Industry Applications Conference, 2006. 41st IAS Annual Meeting. Conference Record of the 2006 IEEE*, vol. 1, pp. 84–89. IEEE, 2006.

[9] A. Videt, M. Messaoudi, N. Idir, H. Boulharts, and H. Vang, "Pwm strategy for the cancellation of common-mode voltage generated by three-phase back-to-back inverters," *IEEE Transactions on Power Electronics*, vol. 32, no. 4, pp. 2675–2686, 2017.

[10] J. Samanes, A. Urtasun, E. Gubia, and A. Petri, "Robust multisampled capacitor voltage active damping for grid-connected power converters," *International Journal of Electrical Power and Energy Systems*, vol. 105, pp. 741–752, 2019.

[11] A. M. Hava, R. J. Kerkman, and T. A. Lipo, "A high-performance generalized discontinuous pwm algorithm," *IEEE Transactions on Industry applications*, vol. 34, no. 5, pp. 1059–1071, 1998.

[12] J. W. Kolar, H. Ertl, and F. C. Zach, "Influence of the modulation method on the conduction and switching losses of a pwm converter system," *IEEE Transactions on Industry Applications*, vol. 27, no. 6, pp. 1063–1075, 1991.

[13] A. M. Hava, R. J. Kerkman, and T. A. Lipo, "Simple analytical and graphical methods for carrier-based pwm-vsi drives," *IEEE transactions on power electronics*, vol. 14, no. 1, pp. 49–61, 1999.

[14] BDEW, "Technical Guideline: Generating Plants Connected to the Medium- Voltage Network," BDEW, Berlin, Germany, 2008.

[15] A. Tcai, H.-U. Shin, and K.-B. Lee, "Dc-link capacitor-current ripple reduction in dpwm-based back-to-back converters," *IEEE Transactions on Industrial Electronics*, vol. 65, no. 3, pp. 1897–1907, 2018.

[16] "Ieee recommended practice for grounding of industrial and commercial power systems," *IEEE Std 142-2007 (Revision of IEEE Std 142-1991)*, DOI 10.1109/IEEESTD.2007.4396963, pp. 1–225, Nov. 2007.

[17] M. Kaufhold, H. Aninger, M. Berth, J. Speck, and M. Eberhardt, "Electrical stress and failure mechanism of the winding insulation in pwm-inverter-fed low-voltage induction motors," *IEEE Transactions on industrial electronics*, vol. 47, no. 2, pp. 396–402, 2000.

[18] J.-W. Choi and S.-K. Sul, "Inverter output voltage synthesis using novel dead time compensation," *IEEE transactions on Power Electronics*, vol. 11, no. 2, pp. 221–227, 1996.

Javier Samanes was born in Pamplona, Spain, in 1990. He received the M.Sc. degree in electrical engineering from the Public University of Navarre (UPNA), Pamplona, Spain, in 2014 and the M.Sc. degree in renewable energy engineering in 2016 from the same institution. He obtained the Ph.D. degree in electrical engineering from the UPNA in 2018.

In 2014, he joined the Electrical Engineering, Power Electronics and Renewable Energy Research Group (INGEPER) at the UPNA, where he is currently Assistant Professor and member of the Institute of Smart Cities (ISC). In 2018 he was visiting scholar in the Center for Power Electronic Systems (CPES) at Virginia Tech, USA. His research interests include power electronics and renewable energies.

Eugenio Gubia received the M.Sc. and Ph.D. degrees in industrial engineering from the Public University of Navarre, Spain, in 1995 and 2003, respectively.

He joined the Electrical and Electronic Department of the Public University of Navarre in 1996, where he is currently an associate professor and member of the Institute of Smart Cities (ISC). In 2002, he joined the Electrical Engineering, Power Electronics, and Renewable Energy Research Group (INGEPER). From June to December 2005, he worked as a guest researcher at the Center for Power Electronics Systems (CPES) in the field of electromagnetic compatibility. His research interests are in the field of power electronics, renewable energy systems, high-frequency phenomena, and electromagnetic compatibility.

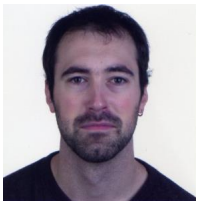

Xabier Juankorena received the M.Sc. degree in electrical engineering in 2008 and the Ph. D. in electrical engineering in 2015, both from the Public University of Navarre, Pamplona, Spain. Since 2012, he has been working as R&D Engineer in the Wind-power Department of Ingeteam. His research interests are in the field of power electronics, wind power systems and control.

Carlos Girones received the M.Sc. degree in electrical engineering in 2003 from the Public University of Navarre, Pamplona, Spain. Currently he has been working as R&D Director in the Wind power Department of Ingeteam. His research interests are in the field of renewable Energy, power electronics and Digital transformation.